applied sciences

MDPI

Article

Design and Optimization of the Bi-Directional U-Ribbed Stiffening Plate–Concrete Composite Bridge Deck Structure

Dingchao Wei [1,†], Jingwen Liao [2,†], Jianjun Liu [1], Yingjie Gao [2] and Fanglin Huang [2,*]

[1] Guizhou Transportation Planning Survey & Design Academe Co., Ltd., Guiyang 550081, China; gzjtsjzp@126.com (D.W.); liujj@gzjtsjy.com (J.L.)
[2] School of Civil Engineering, Central South University, Changsha 410075, China; l2716788092@163.com (J.L.); gyj_812_csu@163.com (Y.G.)
* Correspondence: huangfanglin@csu.edu.cn
† These authors contributed equally to this work.

Abstract: The steel–concrete composite structure is widely used in civil engineering for large-span bridges. Orthotropic steel bridge decks (OSDs) have particularly gained popularity due to their excellent mechanical performance. To address cracking issues in OSDs and concrete in negative moment regions, a novel bi-directional U-ribbed stiffening plate (BUSP)–concrete composite bridge deck is proposed. By using finite element analysis, the mechanical performance is evaluated based on maximum tensile stress and vertical displacement of concrete overlays. Results show that the BUSP–concrete deck outperformed conventional flat decks. It is also found that increasing the height, thickness, and opening width of U-ribs reduced tensile stress and maximum displacement. Adjusting height had the most significant effect on displacement while opening width affected tensile stress the most. Considering material usage, optimizing height is proved to be more effective than adjusting thickness and opening width. Decreasing spacing parameters improved performance but added complexity and reduced construction convenience. These findings will guide the design and optimization of steel–concrete composite bridge deck structures.

Keywords: steel–concrete composite bridge deck; the bi-directional U-ribbed stiffening plate (BUSP); structure optimization and design; parametric analysis; finite element analysis

check for updates

Citation: Wei, D.; Liao, J.; Liu, J.; Gao, Y.; Huang, F. Design and Optimization of the Bi-Directional U-Ribbed Stiffening Plate–Concrete Composite Bridge Deck Structure. *Appl. Sci.* **2023**, *13*, 9340. https://doi.org/10.3390/app13169340

Academic Editor: Laurent Daudeville

Received: 19 July 2023
Revised: 15 August 2023
Accepted: 16 August 2023
Published: 17 August 2023

Copyright: © 2023 by the authors. Licensee MDPI, Basel, Switzerland. This article is an open access article distributed under the terms and conditions of the Creative Commons Attribution (CC BY) license (https://creativecommons.org/licenses/by/4.0/).

1. Introduction

The steel–concrete composite bridge deck system fully utilizes the tensile strength of steel and the compressive strength of concrete [1,2]. It has been widely adopted in the design and construction of various large-span bridges due to its high structural stiffness, lightweight properties, and reduced deflection [3–6]. Over the past several decades, researchers have conducted theoretical and experimental studies [7–10] to verify the excellent performance of the steel–concrete composite bridge deck system during the service life of bridge structures. Among various types of steel–concrete composite bridge deck systems, the orthotropic steel deck (OSD)–concrete structure has been extensively utilized in medium and large-span bridges due to its advantages such as lightweight design, high load-carrying capacity, and fast construction speed [11].

As a part of the bridge deck system, the factory precast OSD also serves as formwork during the pouring of the concrete structure, reducing the need for wet joints in the concrete structure and greatly enhancing construction efficiency and convenience [2]. To achieve its wider application in steel–concrete composite bridge decks, researchers have conducted a series of studies. For example, Sun et al. [12] achieved a lightweight design of OSD through a multi-objective optimization method. However, the U-ribs stiffeners of the OSD are connected to the panels through welding, resulting in a sudden change in stiffness at the weld joint [13,14]. Consequently, significant stress amplitudes occur at the weld joint, making it susceptible to fatigue cracking under repeated vehicular loading.

To assess the fatigue strength of welds in OSD, Masafumi et al. [15] proposed a novel method for evaluating the root stress of welds. Existing studies have shown that the fatigue performance issues at the welds of OSD greatly affect the service life of bridges and have been a major concern in the implementation of OSD in bridges [13,16–21].

Presently, two methods have been proposed to improve the fatigue performance of the deck-to-rib welded joint in OSD. Firstly, it is reported to enhance the strength of the weld by employing techniques such as double-sided welding [22,23] and deep-penetration welding [24], which, however, impose higher demands on welding technology [25]. Secondly, increasing the thickness (or rigidity) of the bridge deck panel can significantly reduce stress amplitudes in the bridge deck structure, which can be achieved by using rigid cement-based materials [26–28] or ultra-high-performance concrete (UHPC) [11]. Meanwhile, Alireza [29] investigated the feasibility of using UHPC in bridge deck areas through experimental and numerical simulation methods. However, implementing such solutions not only increases the cost of bridge construction but also fails to address the issue of geometric discontinuity at the weld joint between the deck and the U-ribs of OSD [25].

In recent years, a corrugated steel–concrete composite bridge deck (CSCCBD) system comprising concrete, corrugated steel plates, and perforated plate shear connectors has been implemented in bridge constructions [30]. This bridge deck system replaces U-ribs with continuous corrugated steel, eliminates the decks of OSD, and replaces them with cast-in-place concrete panels. This effectively resolves issues arising from abrupt stiffness variations at the weld joint between the OSD panel and U-ribs. Extensive research has been conducted to investigate various aspects of the performance of the CSCCBD system to promote its application in bridge structures. Kim et al. [30] conducted pull-out experiments to validate the significant role of shear connectors in CSCCBD. Jeong et al. [31] investigated the ultimate bearing capacity of CSCCBD and proposed a simplified calculation formula for predicting it. Kong et al. [1] studied the influence of variation in shear connectors on the slip performance of CSCCBD. However, most existing research has primarily focused on the impact of variations in the internal structure of CSCCBD, such as different sizes or structural configurations of shear connectors. In fact, like OSD [32–34], the size of corrugated plates (height, thickness, opening width, etc.) also influences the mechanical performance of CSCCBD, posing an intriguing question worthy of exploration.

This study presents a novel bi-directional U-ribbed stiffening plate (BUSP)–concrete composite bridge deck system, which combines the advantages of continuous placement of U-ribs as in CSCCBD with the avoidance of welded connections between U-ribs and steel plates, thereby enhancing the lateral stiffness of the bridge deck system, exhibiting superior resistance to eccentric bridge deck loading. Moreover, to address the difficulties in positioning and installing rebars within the PBL shear connector groups (a commonly used type of shear connector in CSCCBD) [1], improvements have been made to the conventional PBL shear connectors in the innovative BUSP–concrete composite bridge deck system. The openings of the new type of PBL shear connectors extend to the bottom of the BUSP, and after concrete pouring, these openings are filled. This approach effectively enhances the longitudinal shear resistance between the concrete and steel structures.

In this paper, a parameterized modeling script for ABAQUS was developed based on Python. The script considers five size parameters, including the height, thickness, and opening width of a single U-rib in BUSP, as well as the transverse and longitudinal spacing between U-ribs. Based on an actual bridge in Guizhou Province, China, a structural finite element model of the BUSP–concrete composite bridge deck was established. The study aims to comprehensively investigate the influence of size parameter variations on the mechanical performance of BUSP–concrete composite bridge deck structures. Furthermore, the combined variations of multiple size parameters will be compared to assess the extent of their impact on structural performance. The research findings of this study will provide valuable insights into the design and application of novel BUSP–concrete composite bridge deck structures.

2. Research Background

The bridge under study is in Guizhou Province, China, and spans a total length of 381.5 m. It has a main span measuring 280 m and a deck width of 38.9 m. The upper portion of the main bridge is composed of a steel-reinforced concrete truss arch section with a clear span of 260 m, as depicted in Figure 1. The bridge deck is constructed using a composite beam structure comprised of steel crossbeams and concrete overlays. The plan view of the crossbeams is depicted in Figure 2.

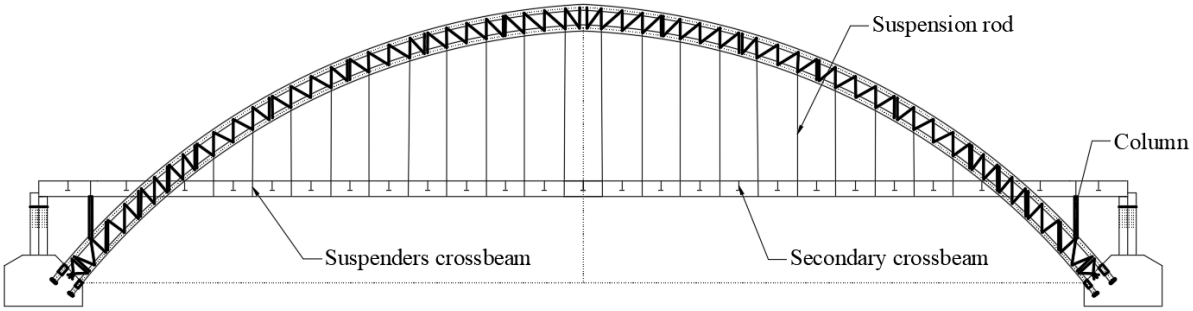


Figure 1. Bridge Elevation Drawing.

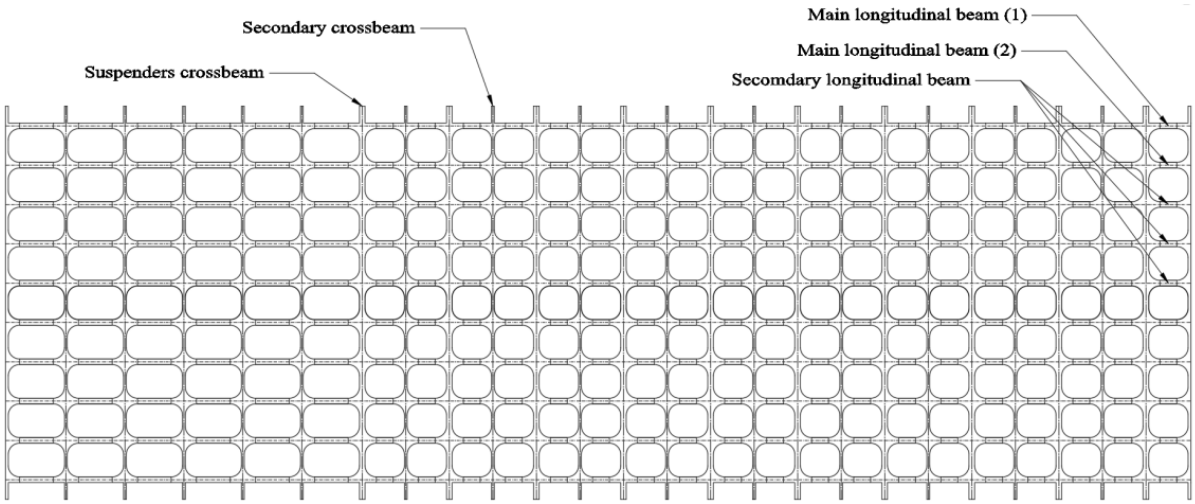


Figure 2. Plan View of Transverse and Longitudinal Beams.

3. Structural Design and Optimization

3.1. Optimization of Element Partitioning

The planned construction approach for the concrete structure of the bridge in this study involves factory prefabrication. However, this method requires favorable transportation conditions and sufficient space for material storage. Additionally, the prefabricated elements necessitate a prolonged curing process, leading to increased construction duration and cost. To address these challenges, this paper proposes the incorporation of steel panels into the bridge deck. These panels serve a dual purpose: acting as permanent structural elements of the bridge deck and serving as formwork during the cast-in-place construction of the concrete structure.

Furthermore, the addition of steel panels increases the steel consumption in the bridge deck system. To maintain the overall steel quantity, an optimization of the crossbeam system is proposed. To achieve an optimized calculation of the overall structure, the bridge deck system is divided into elemental units. The segmented local units are then treated as the design objects instead of considering the entire bridge.

A finite element (FE) model is established using the crossbeams of the bridge deck system and the concrete overlays. The model incorporates symmetry simplifications. For

the transverse direction, the FE model represents half of the total transverse span of the bridge, while for the longitudinal direction, it corresponds to the length between the transverse beams of the three suspension rods, as shown in Figure 3.

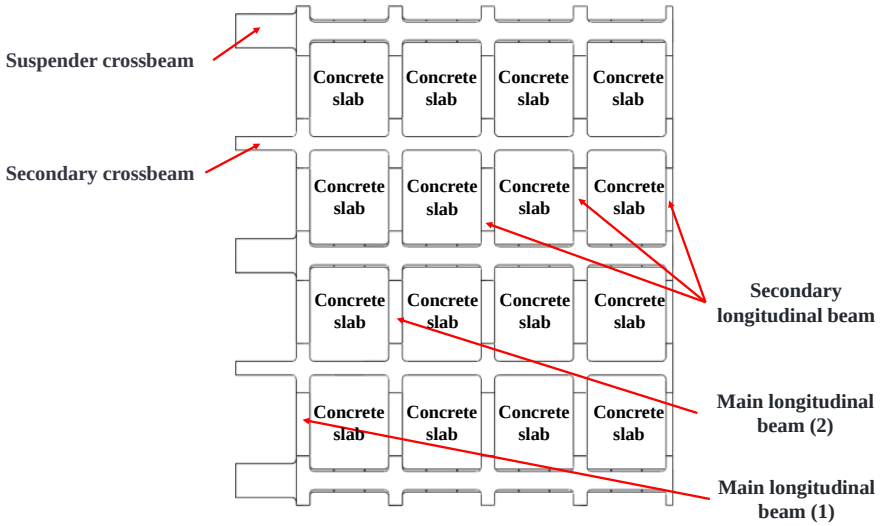


Figure 3. Schematic diagram of local optimization units.

3.2. Design and Optimization of Structures

Three-dimensional models of the structure are established; the original scheme is depicted in Figure 4. The improved configuration, when compared to the original scheme, introduces several changes. First, it eliminates the secondary crossbeams between the suspender crossbeams. Second, a layer of 10 mm-thick ordinary steel plate is added on top of the crossbeams. This steel plate serves multiple purposes—it acts as a protective layer and provides additional strength to the bridge deck.

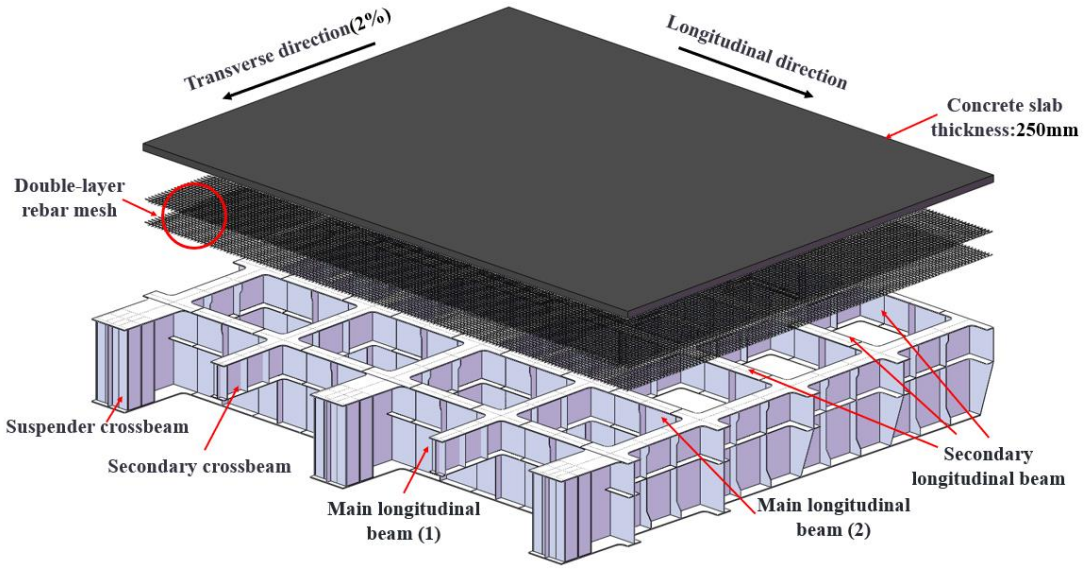


Figure 4. The schematic diagram of the three-dimensional model of the original scheme.

To ensure proper connection between the concrete and steel structures, improved PBL shear connectors are employed at the top of the steel plate. These connectors not only enhance the anti-slip capability but also replace the longitudinal steel bars used in the original scheme. This replacement partially compensates for the increased steel consumption resulting from the addition of the ordinary steel plate.

Figure 5 illustrates the improved configuration, showcasing the absence of secondary crossbeams and the inclusion of the steel plate. On the other hand, Figure 6 depicts the design of the improved PBL shear connectors.

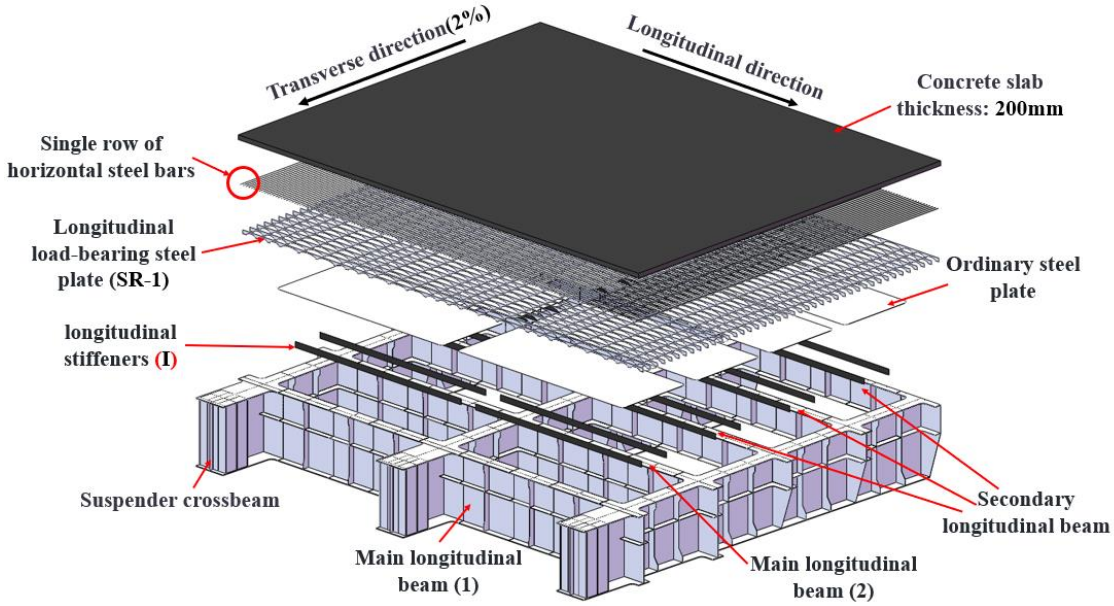


Figure 5. The three-dimensional schematic diagram of the improved configuration.

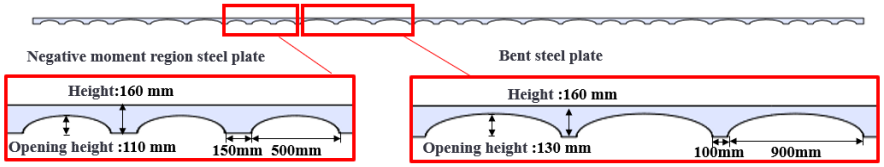


Figure 6. The schematic diagram of the improved PBL shear connectors in the optimized configuration of the ordinary steel plate scheme.

To analyze the structural response of the two configurations, FE models were created using the 2020 ABAQUS software. The steel bars were represented using one-dimensional truss elements (Truss), while solid elements (C3D8R) were utilized for the remaining parts of the model. The details of the model establishment are shown in Table 1.

Table 1. The details of model establishment.

Materials	Structures	Young's Modulus (GPa)	Poisson's Ratio	Type of Meshes	Size of Meshes (mm)
Concrete	Concrete overlay	34.5	0.2	C3D8R	150
Steel	Rebar	206	0.3	Truss	150
	PBL shear connectors	206	0.3	C3D8R	150
	Stiffening rib	206	0.3	C3D8R	150
	Steel beam	206	0.3	C3D8R	150

Hinge boundary conditions were applied to one end of the suspender crossbeams, while symmetric boundary conditions were applied to the other end. This setup allows for appropriate modeling of the structural behavior. In terms of loading, the concrete slab was subjected to a design load that is 1.2 times the load of a class-I highway vehicle. This

loading condition allows for a realistic simulation of the expected forces on the bridge. Table 2 presents the results obtained from the analysis, including the maximum tensile stress and vertical displacement of the concrete overlays, as well as the maximum stress and vertical displacement of the steel structures.

Table 2. Comparison between the original scheme and the improved scheme.

Scheme	Stress (MPa)		Displacement (mm)		Material Consumption	
	Concrete	Steel	Concrete	Steel	Concrete (m^3)	Steel (t)
Original Scheme	1.28	63.81	4.95	7.01	92.96	161.50
Optimization Scheme	0.91	56.77	4.15	6.45	74.37	162.81
Amplitude of Variation (%)	−28.91	−11.03	−16.16	−7.99	−20.00	0.81

According to Table 2, it can be observed that the improved design scheme effectively reduces the stress and displacement amplitudes of the structure without a significant increase in steel consumption, with a concrete saving of up to 20%. Furthermore, by altering the construction method of the concrete structure, it will effectively decrease construction costs and alleviate construction difficulty.

3.3. BUSP Design

In continuation of the improved structural configuration, this study introduces further optimization by proposing a novel bi-directional U-ribbed stiffening plate (BUSP) for the top of the crossbeam system. The BUSP is designed to enhance the structural performance of the bridge deck. The modeling is done in the same way as other steel components, such as steel beams. To complement the implementation of the BUSP, adjustments are made to the PBL shear connectors. These modifications are aimed at ensuring proper integration and compatibility between the BUSP and the PBL shear connectors.

Figure 7 provides an illustration of the proposed BUSP, and Figure 8 provides the adjusted PBL shear connectors, showcasing their design and arrangement. Table 3 presents a comparison between the computational results of the BUSP scheme and the original scheme. This comparison aims to evaluate the performance and effectiveness of the proposed BUSP configuration in contrast to the original configuration.

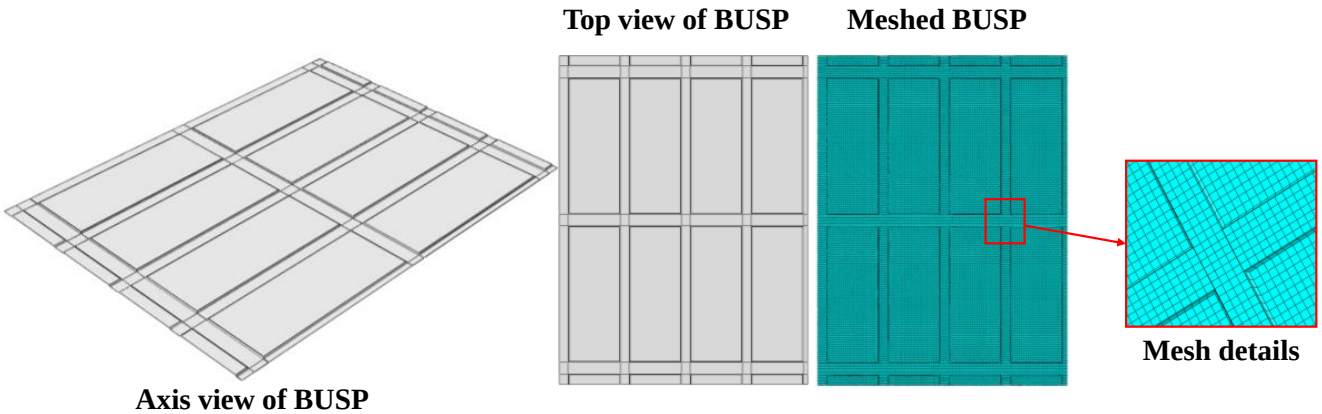
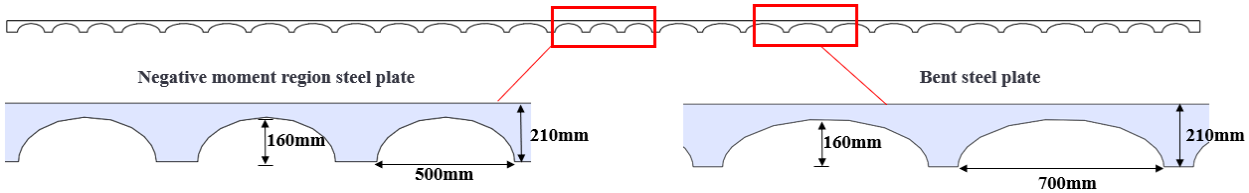
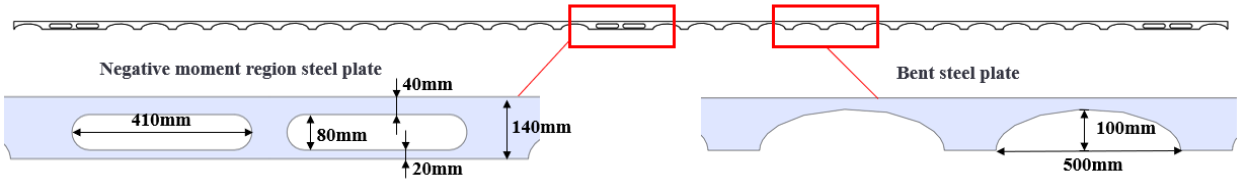


Figure 7. Schematic illustration of BUSP.



(**a**) SR-2



(**b**) SR-3

Figure 8. The schematic diagram of the improved PBL shear connectors in the optimized configuration for the BUSP scheme.

Table 3. A comparative analysis between the original scheme and the BUSP scheme.

Scheme	Stress (MPa)		Displacement (mm)		Material Consumption	
	Concrete	Steel	Concrete	Steel	Concrete (m^3)	Steel (t)
Original Scheme	1.28	63.81	4.95	7.01	92.96	161.50
BUSP Solution	0.90	56.88	3.87	6.29	75.16	163.51
Amplitude of Variation (%)	−29.69	−10.86	−21.82	−10.27	−19.15	1.24

Based on the information provided in Table 3, it is evident that the adoption of the BUSP solution yields significant improvements compared to the original scheme. The displacement of the concrete overlays is reduced by 10.27% when using the BUSP configuration. Additionally, there is a notable decrease of 29.69% in the maximum tensile stress experienced by the structure.

These findings demonstrate that the implementation of the BUSP effectively enhances the stiffness and performance of the concrete structure within the bridge deck system. The BUSP solution proves to be successful in mitigating displacement and reducing tensile stress, indicating its potential as an effective design modification for improved structural performance.

4. Parametric Study by Computational Analysis

4.1. Computation Model

To investigate the impact of size parameters of the bi-directional U-ribbed stiffening plate (BUSP) on structural stress, finite element analysis (FEA) models were constructed for a portion of the bridge using the ABAQUS software. Two types of structural models were primarily established for this analysis.

Both types of models incorporated the U-ribbed stiffening plate, which is depicted within the black box in Figure 9. The key difference between the two models lies in the crossbeams used. Structure 1 utilized optimized crossbeams, while Structure 2 retained the crossbeams from the original design. The purpose of creating these two variations of computational models is to further validate the effectiveness of the optimized crossbeams. Additionally, the computational results obtained from the two types of FEA models, with different size parameters, will be compared with the original structure.

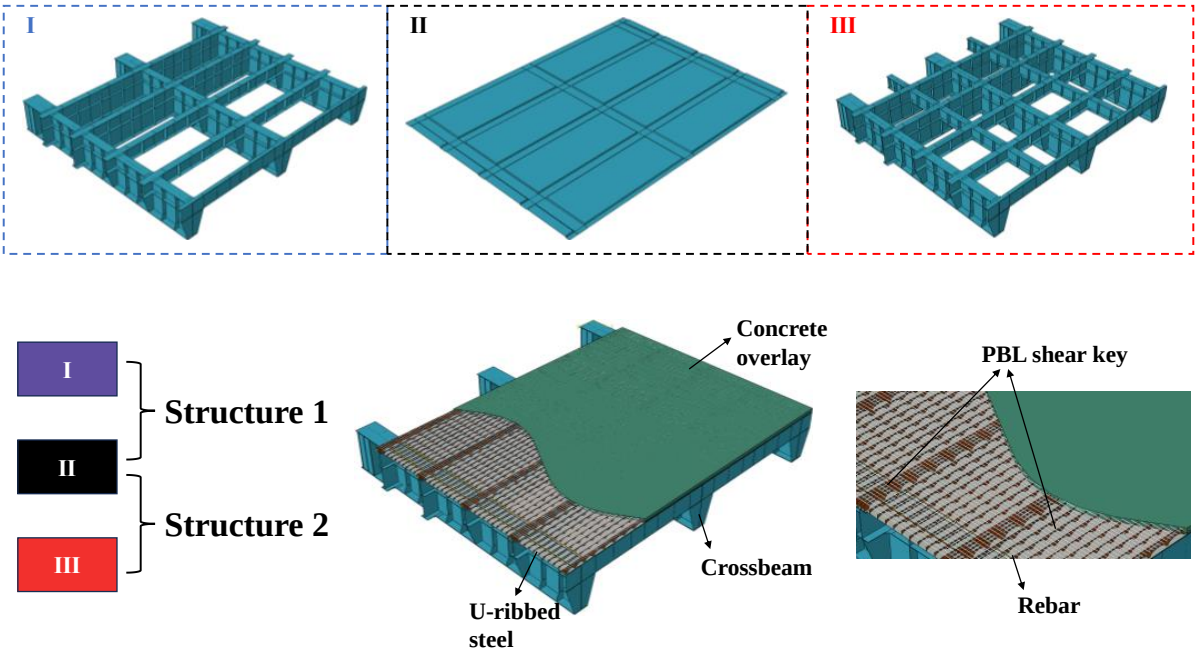


Figure 9. Configuration of a structural model.

In the U-ribbed stiffening plate, the size parameters include both individual U-rib characteristics and various spacing parameters between U-ribs. The size parameters of a single U-rib consist of the following: the height of the U-rib (h), the opening width of the U-rib (a), the bottom width of the U-rib (b), the thickness of the steel plate (t), and the angle between the side and bottom edges of the U-rib (α). On the other hand, the spacing parameters between U-ribs comprise the spacing between longitudinal U-ribs along the transverse direction of the bridge (e) and the longitudinal spacing between transverse U-ribs (w). The meaning of these size parameters is shown in Table 4. And all these size parameters used in the FEA models are illustrated in Figure 10 for reference.

Table 4. The meaning of the size parameters for the U-ribbed stiffening plate.

Parameters	Meaning
h	The height of the U-rib
a	The opening width of the U-rib
b	The bottom width of the U-rib
t	The thickness of the steel plate
α	The angle between the side and bottom edges of the U-rib
e	The spacing between longitudinal U-ribs
w	The spacing between transverse U-ribs

In a single U-rib of the BUSP, there are five size parameters: a, b, α, h, and t. However, these parameters are not entirely independent. For instance, when b is kept constant, changing the value of a will correspondingly affect the value of α. This relationship between a, b, and α indicates that α is a non-independent parameter. Furthermore, since the bottom of the BUSP directly contacts the crossbeams, the size of the U-rib's bottom (b) must be consistent with the flange plate dimensions of the crossbeams. Therefore, the primary focus of this paper regarding the single U-rib size parameters is on a, h, and t. The parameter b has been set as a constant value of 600 mm, matching the dimensions of the crossbeam flange.

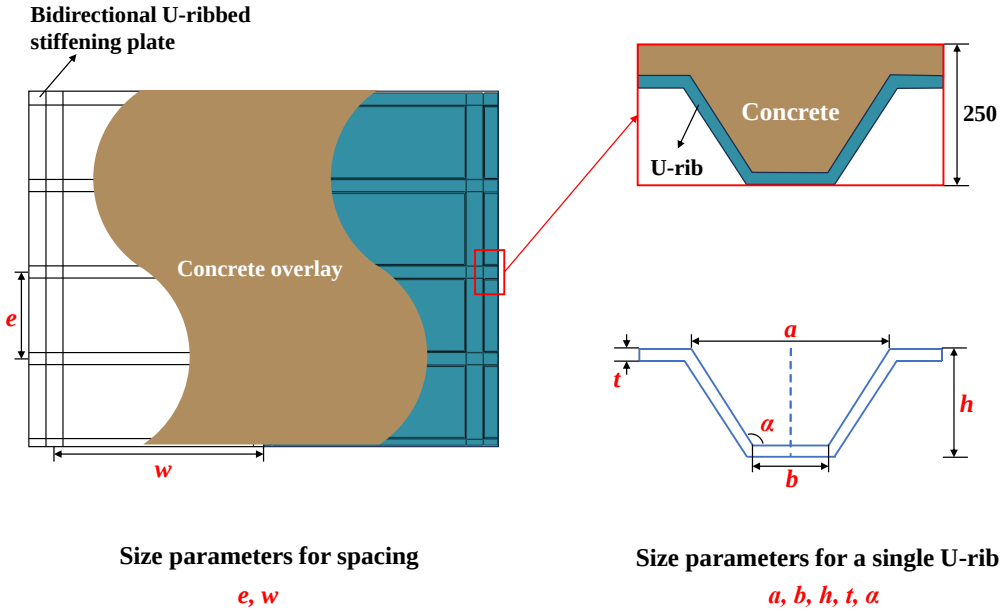


Figure 10. Size parameters of the BUSP (unit: mm).

When discussing the single U-rib size parameters, the spacing size parameters, e and w, were set as 4112.5 mm and 10,000 mm, respectively. This setting aims to achieve compatibility between the bottom side of the BUSP and the crossbeams.

Once all the size parameters are determined, the coordinates of each node on the BUSP can be calculated using geometric methods. A Python script was developed for ABAQUS to facilitate the process of parametric modeling. In this script program, the nodes of the U-rib are assigned numerical labels, as shown in Figure 11, with Node 1 serving as the origin of the coordinate system. In the case that the nodes of the U-rib have been processed according to Figure 11, the coordinates of all the U-rib nodes can be expressed as a function of the size parameters. Table 5 presents the x-coordinates (abscissa) and y-coordinates (ordinate) for the eight nodes of the U-rib, in which c is calculated according to the following formula.

$$c = |t/\tan(\alpha/2)| \quad (1)$$

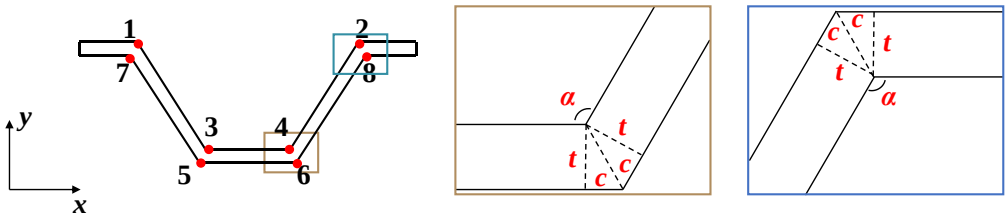


Figure 11. Node numbering of U-rib.

Table 5. The abscissa and ordinate of the nodes of the U-rib.

Node Number	x (mm)	y (mm)
1	0	0
2	a	0
3	$(a-b)/2$	$t-h$
4	$(a+b)/2$	$t-h$
5	$(a-b)/2-c$	$-h$
6	$(a+b)/2+c$	$-h$
7	$-c$	$-t$
8	$a+c$	$-t$

In the context of bridge structures, one common type of deck distress is the cracking and failure of the concrete overlay due to excessive tensile stress. These cracks can also lead to water infiltration, which in turn causes corrosion of the underlying steel structure. This deterioration significantly impacts the service life of the bridge structure. Therefore, the focus of this study is to investigate the variations in stresses and displacements of the concrete overlay when different values are assigned to the three independent parameters (a, h, and t).

By examining how these parameters affect the behavior of the concrete overlay, we can gain insights into the potential causes of cracking and failure. This knowledge can then be used to develop strategies for improving the design and maintenance of bridge structures, ultimately enhancing their durability and extending their service life.

4.2. Influence of Single Parameters h, t, and a

Indeed, the height of the U-rib (h) plays a crucial role in the design of the BUSP. Using a simple rectangular section beam as an example, its bending stiffness is directly proportional to the cube of its height. This example clearly illustrates that the distribution of material along the height direction significantly impacts the bending resistance of structures. To explore this further, this paper considers values of 70, 80, 90, 100, and 110 mm for h.

Figure 12 demonstrates that variations in h have a more pronounced effect on the bending stiffness of the U-rib compared to changes in t and a. Increasing h effectively increases the bending stiffness of the BUSP. However, it is important to note that an increase in h does not necessarily result in smaller concrete stresses. Figure 13 provides information on the maximum stress and displacement of the concrete overlay in Structure 1, Structure 2, and the original structure for different values of h (70, 80, 90, 100, and 110 mm). Additionally, Figure 13c compares the stress of the steel crossbeams in Structure 1 and Structure 2 with that of the original structure.

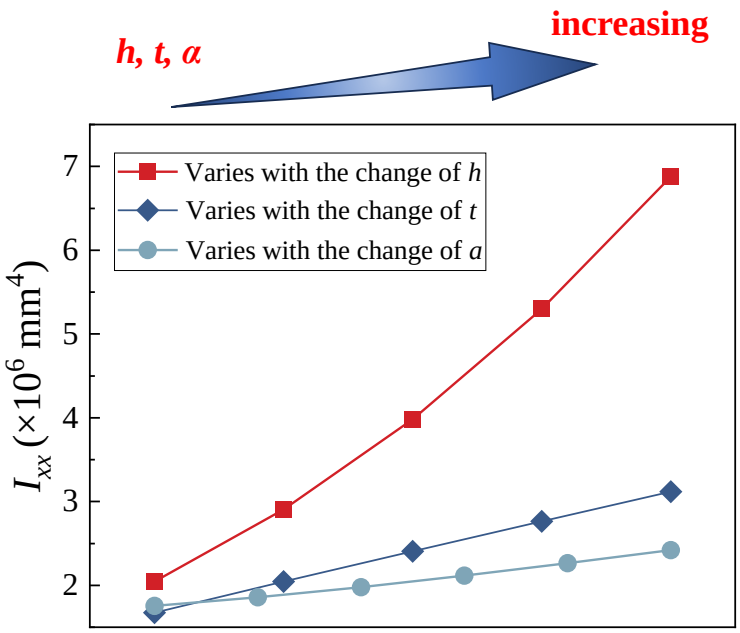


Figure 12. The bending stiffness of the U-rib varies with the change of h, t and a.

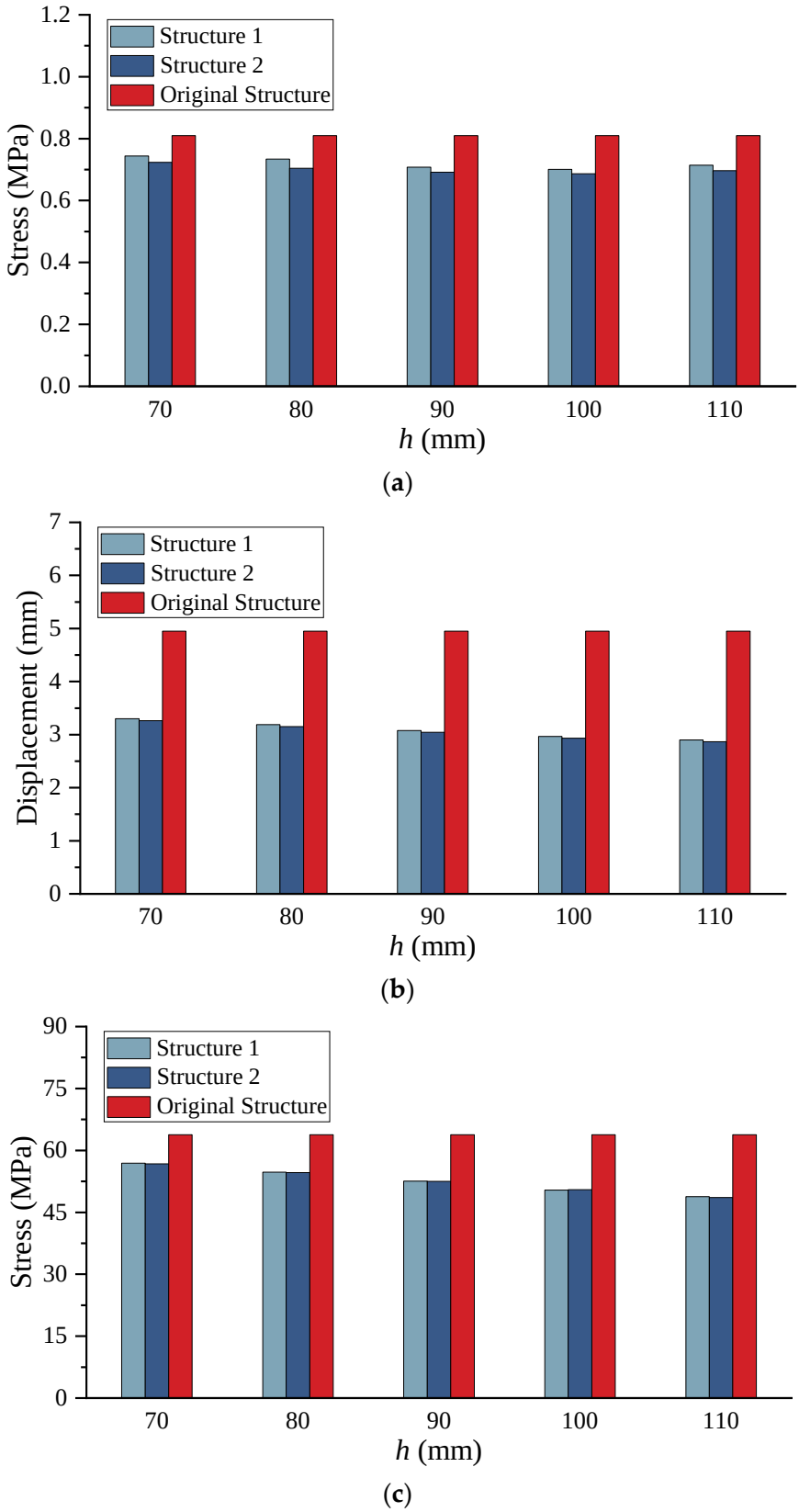


Figure 13. The impact of changes in the *h* value on the bridge deck structure: (**a**) impact on stress of concrete overlay, (**b**) impact on displacement of concrete overlay, (**c**) impact on stress of crossbeam.

These figures provide insights into how variations in h affect the internal stresses and displacements of the concrete overlay and the steel crossbeams. By analyzing these results, we can better understand the impact of parameter changes on the structural behavior and determine optimal design configurations for the BUSP.

From the observation of Figure 13, it is evident that both Structure 1 and Structure 2 exhibit significant improvements in strength and stiffness when compared to the original structure. This improvement is primarily characterized by lower displacement and stress levels in the concrete overlay under the same load conditions, as well as enhanced stress in the steel crossbeam.

Following the principle of a single variable, except for the height change of the U-rib, all other size parameters remain constant. By examining the graph in Figure 13, it can be seen that, except for the transition from 100 mm to 110 mm, the displacement, and stress of the concrete overlay increase as the height decreases under the five specified h values. Referring to Figure 10, it is noted that the total thickness of the concrete overlay, including the U-ribs, is 250 mm. Consequently, an increased h value leads to thinner sections without U-rib stiffeners in the concrete overlay, which could have an unfavorable impact on the stress distribution in those areas.

In the range of h values between 70 mm and 100 mm, the reinforcement provided by the U-ribs mitigates this adverse effect to some extent. However, when the height of the U-ribs reaches 110 mm, this effect becomes more pronounced. Thus, for the BUSP, a larger h value does not necessarily translate to improved performance.

Based on these findings, it is crucial to strike a balance between the height of the U-ribs and the overall design objectives of the BUSP. Simply increasing the height without considering the corresponding effects on stress distribution and performance might not yield the desired outcome. Therefore, careful consideration should be given to selecting an optimal h value during the design process.

Based on the observation of Figure 12, increasing the value of t (thickness) is more advantageous in enhancing the stiffness of the BUSP compared to increasing the value of a (width). This is attributed to the fact that both t and h (height) are dimensions in the vertical direction, thus influencing the bending stiffness of the structure. To assess the impact of variations in t on the performance of the BUSP, calculation models were created for the BUSP using different t values: 8 mm, 10 mm, 12 mm, 14 mm, and 16 mm. Figure 14 depicts the stress and displacement of the concrete overlay for the three structures under these specified t conditions. From the analysis of Figure 14, it is apparent that both the maximum stress and displacement of the concrete overlay decrease as the t value (thickness) increases. When t is increased from 8 mm to 16 mm, the range of variation in maximum stress within the concrete overlay is almost equivalent to the range observed when h (height) is increased from 70 mm to 110 mm. While increasing the t value can enhance the stiffness of the BUSP, it also leads to a significant increase in the amount of steel required. This implies that there would be a corresponding rise in construction costs and material consumption.

From the analysis of Figure 15, it is evident that both for a single U-rib and for the BUSP, the increase in steel consumption caused by increasing the t value (thickness) is significantly greater than the effects of changes in h (height) and a (width) values. This suggests that increasing the height of the U-ribs in the BUSP is a more effective approach for managing tensile stress in the concrete overlay compared to thickening the BUSP. By focusing on increasing the height of the U-ribs, it is possible to improve the structural performance and control stresses without significantly escalating the steel consumption or construction costs associated with the thickening of the entire BUSP.

This information highlights the importance of considering different design parameters and their respective effects on the performance and cost of the structure. Designers should prioritize the most effective and efficient strategies to achieve the desired objectives while optimizing resources and meeting project requirements.

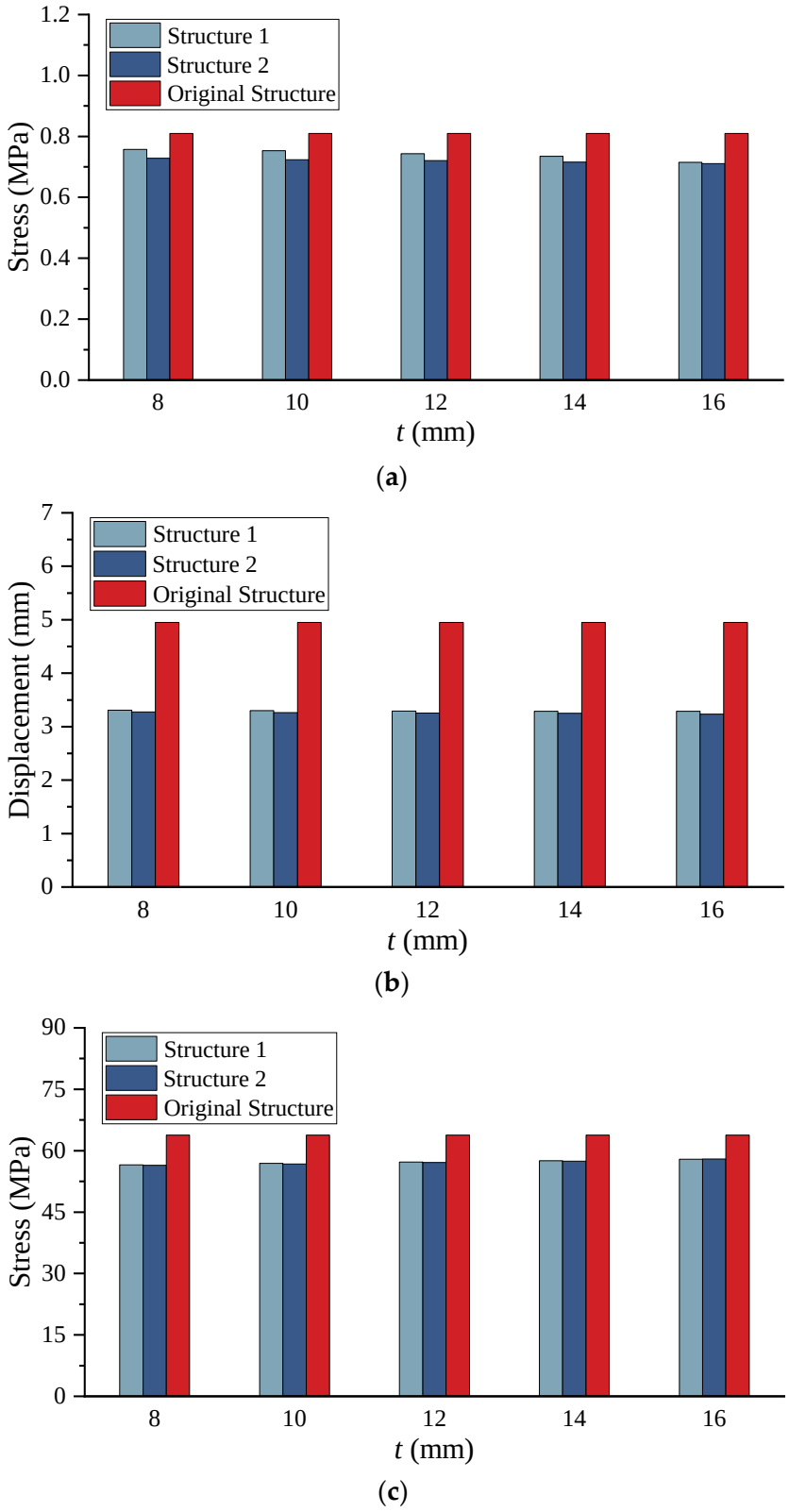


Figure 14. The impact of changes in the *t* value on the bridge deck structure: (**a**) impact on stress of concrete overlay, (**b**) impact on displacement of concrete overlay, (**c**) impact on stress of crossbeam.

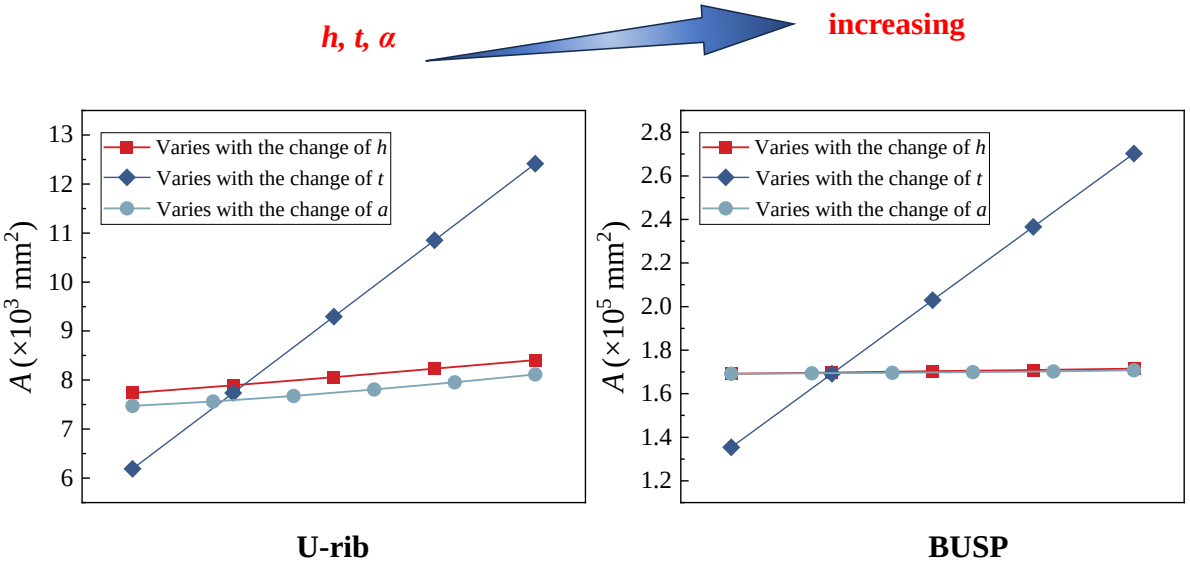


Figure 15. U-rib and BUSP areas vary with changes in *h*, *t*, and *a*.

In addition, six different values of *a* (width), namely 650 mm, 670 mm, 690 mm, 710 mm, 730 mm, and 750 mm, were considered to study their influence on the stiffness of BUSP. Although Figure 12 indicated that varying width values could not effectively enhance the stiffness of the BUSP, changes directly affect the width of the U-shaped stiffeners at the bottom of the concrete overlay, thus increasing its bending stiffness.

In Figure 16, it is evident that increasing the value of *a* leads to a significantly greater increase in the stiffness of the concrete components compared to the other two parameters (*t* and *h*). Additionally, as the value of *h* increases, the flexural stiffness of the concrete component decreases, which explains why the maximum tensile stress in the concrete increases when the *h* value is raised from 100 mm to 110 mm. The decrease in the stiffness of the concrete overlay with an increasing *h* value mainly results from the reduction in the thickness of the concrete overlay outside the U-ribs.

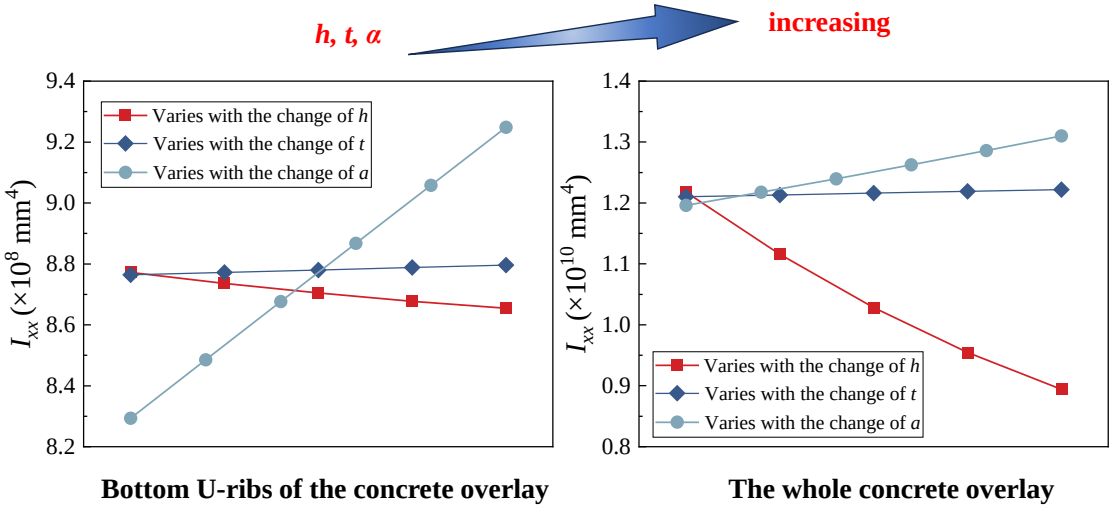
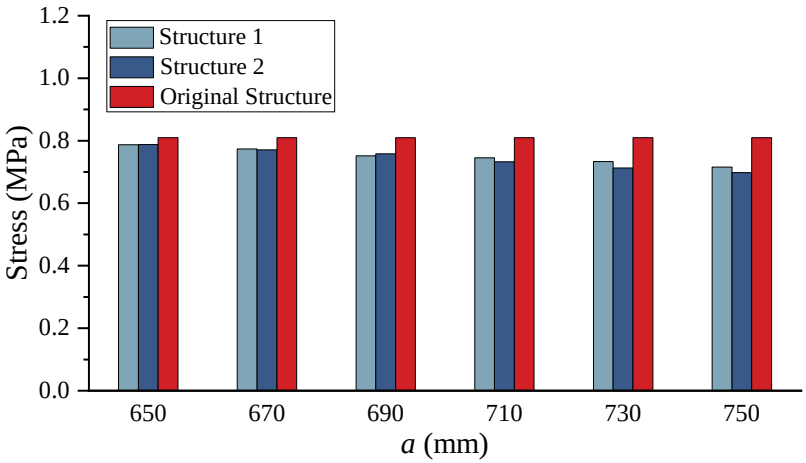


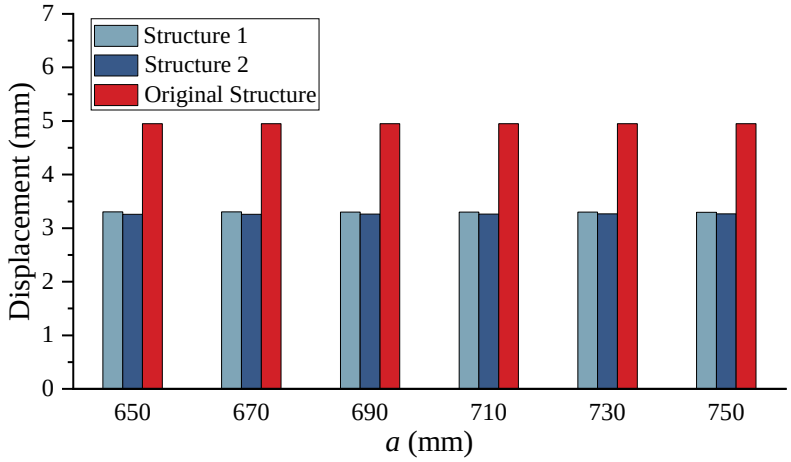
Figure 16. The stiffness of the concrete varies with changes in *h*, *t*, and *a*.

These findings emphasize the importance of considering different design parameters and their respective effects on the stiffness and performance of the concrete components in BUSP structures. Designers should carefully evaluate the trade-offs between different parameters to optimize the overall structural design.

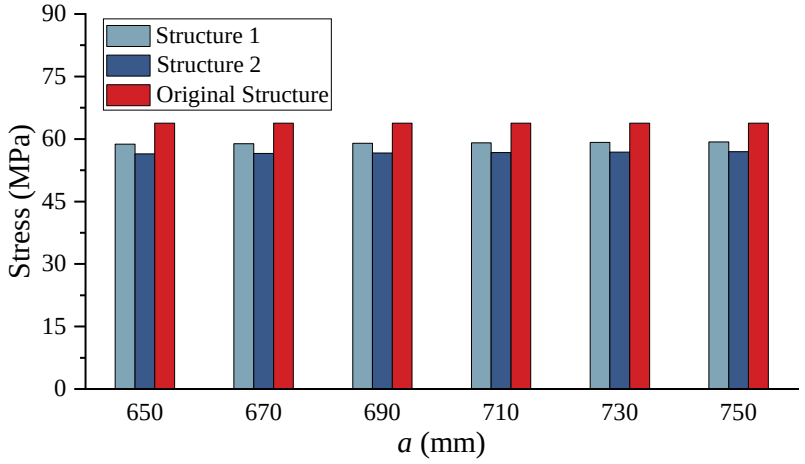
Figure 17 demonstrates that increasing the value of a (width) leads to a decrease in stress and displacement in the concrete overlay, as well as the stress in the steel crossbeam. By increasing the values of h (height) to 100 mm, t (thickness) to 16 mm, or a to 750 mm, it is possible to control the maximum tensile stress of the concrete overlay at approximately 0.71 MPa.



(**a**)



(**b**)



(**c**)

Figure 17. The impact of changes in the a value on the bridge deck structure: (**a**) impact on stress of concrete overlay, (**b**) impact on displacement of concrete overlay, (**c**) impact on stress of crossbeam.

However, it should be noted that just as a larger t value means more steel consumption, increasing the value of a will also result in greater consumption of concrete. Figure 18 illustrates how changes in h, t, and a affect the cross-sectional area of the concrete overlay. Increasing both a and t values will moderately increase the consumption of concrete while increasing the h value will significantly reduce the consumption of concrete. Additionally, increasing the h value will not have a significant impact on the amount of steel used.

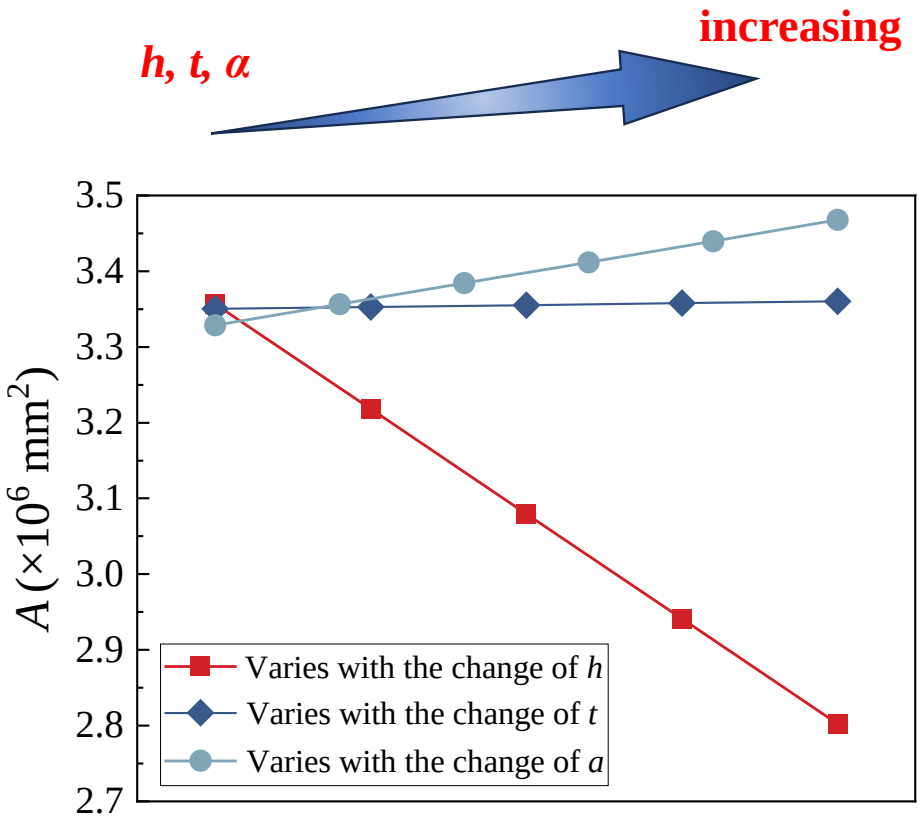


Figure 18. The cross-sectional area of the concrete overlay varies with changes in h, t, and a.

Therefore, among the three discussed size parameters (h, t, and a), controlling the h value appears to be the most effective method for the parameterized design of the BUSP structure in terms of both safety and economy. However, it is important to ensure that the h value is not excessively high, as this would result in a thin concrete overlay that may not meet the design requirements for crack resistance.

Thus, a careful balance needs to be struck between optimizing the size parameters to achieve the desired structural performance while considering material consumption and meeting design standards for concrete durability.

4.3. Coupled Effect of Two or More Parameters in h, t, and a

To further investigate the impact of the three parameters h, t, and a on the design of the BUSP structure for enhancing the stress performance of the concrete overlay in the bridge deck, a parameterized analysis will be conducted in this study. The analysis will involve simultaneous variations of t and h, h and a, and t and a. Firstly, we focus on the simultaneous variation of h and t. Figure 19 illustrates how the stress and displacement of the concrete overlay change with different h and t values. In the figure, stress is represented by the black frame, while displacement is denoted by the red frame.

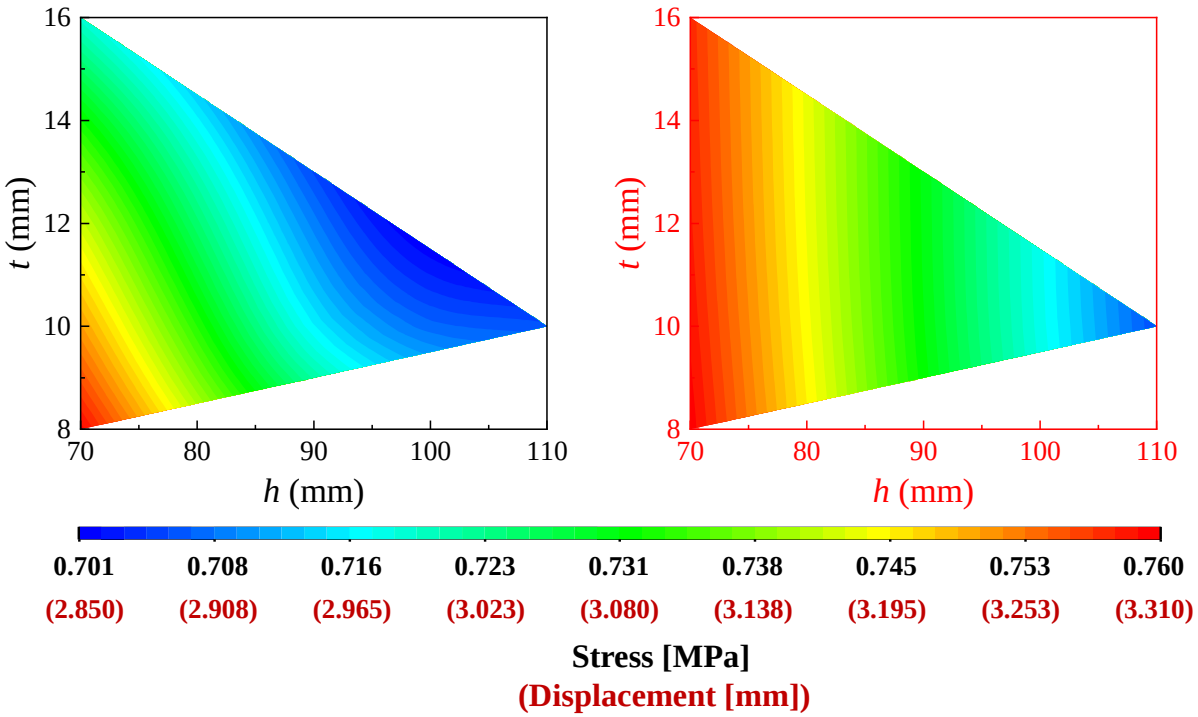


Figure 19. The stress and displacement of concrete overlay vary with the variation of h and t.

As seen in Figure 19, the variation of h and t values exhibit similar effects in improving the maximum tensile stress of the concrete overlay (when the value is smaller than 100 mm). This characteristic is evident from the diagonal trends observed in the stress reduction of the concrete overlay. However, when it comes to their influence on displacement, h and t exhibit different patterns. While both h and t contribute to a decrease in displacement, the impact of h is significantly greater than that of t. This is visually apparent from Figure 19, where the direction of displacement reduction primarily aligns parallel to the h axis.

These findings indicate that adjusting the values of h and t can effectively enhance the stress performance of the concrete overlay in the bridge deck. However, it is worth noting that there may be limitations or optimal ranges for these parameters to ensure structural integrity and crack resistance in the concrete overlay.

Similar to the simultaneous variation of h and t, Figure 20 illustrates the changes in stress and displacement of the concrete overlay with variations in h and a. Comparing Figure 20 with Figure 19 reveals that while an increase in h, t, and a leads to a decrease in the stress of the concrete overlay (when h is below 100 mm), their individual impacts on concrete stress differ. When comparing the variations with h, the direction in which the stress decreases most rapidly, as depicted in Figure 19, is closer to the h-axis, whereas in Figure 20, it is closer to the a-axis. This indicates that variations in t have a slightly smaller effect on the stress of the concrete overlay compared to variations in h, while variations in a have a slightly greater effect.

When considering simultaneous variations of h and a, the trend of maximum vertical displacement of the concrete follows a similar pattern as when considering simultaneous variations of h and t. This implies that among the three parameters adjusting the value of h is the most effective in reducing the vertical displacement of the concrete overlay.

These observations suggest that optimizing the values of h, t, and a can effectively enhance the stress performance and reduce displacement in the concrete overlay of the bridge deck. However, further analysis and evaluation are necessary to determine the specific optimal ranges for these parameters that strike a balance between stress reduction, displacement control, and other design requirements for the BUSP structure.

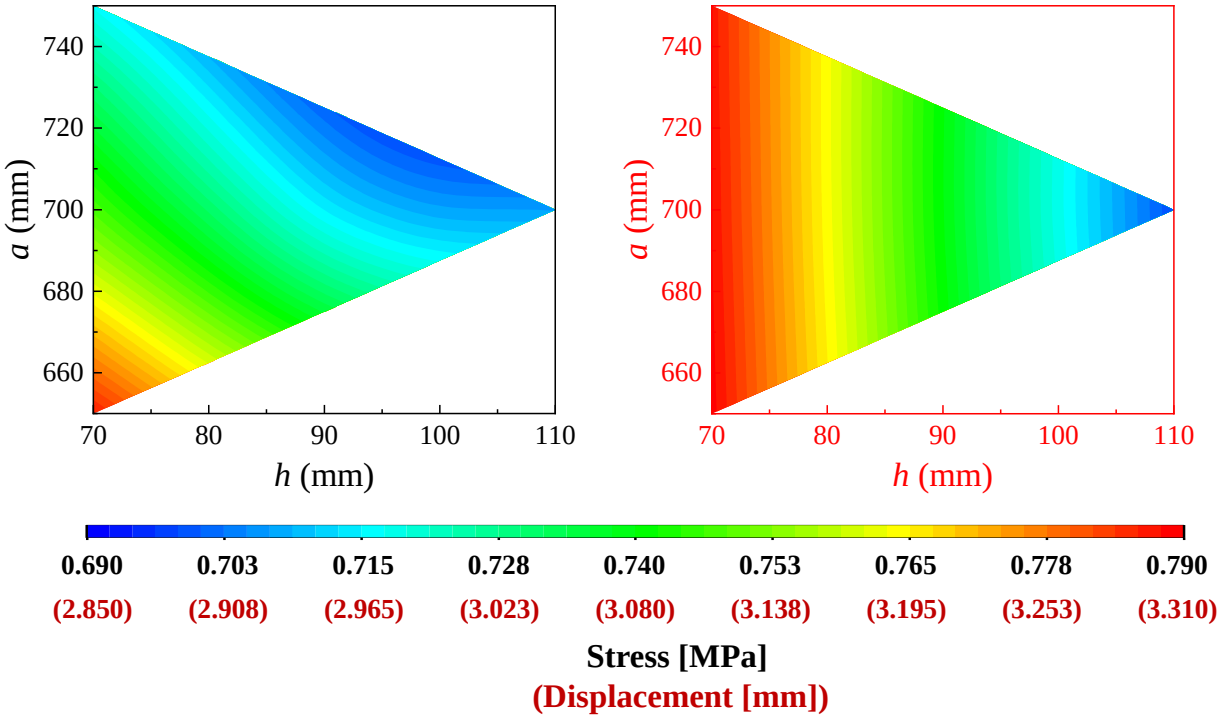


Figure 20. The stress and displacement of concrete overlay vary with the variation of h and a.

Figure 21 illustrates the relationship between the stress and displacement of the concrete overlay and the variations in parameters t (thickness) and a (another parameter). Upon analyzing Figure 21, it becomes apparent that the variation in parameter a primarily affects the maximum tensile stress experienced by the concrete overlay. Conversely, the variation in parameter t has a more pronounced influence on the maximum vertical displacement of the concrete overlay.

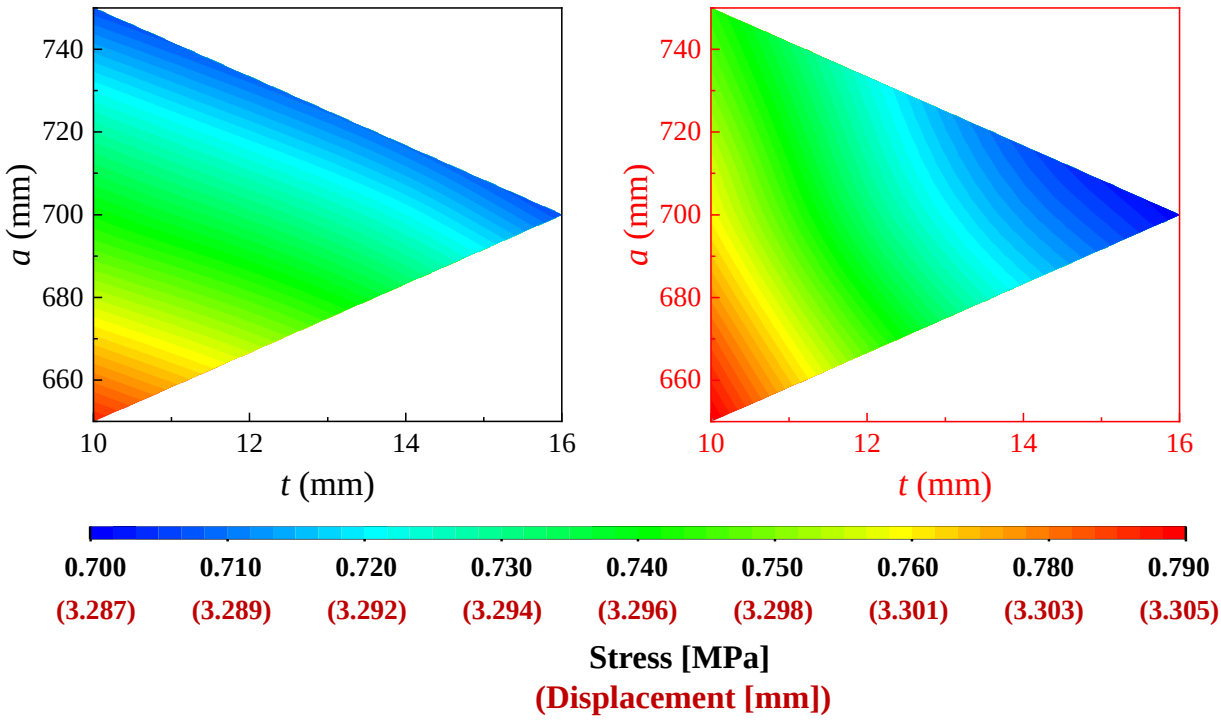


Figure 21. The stress and displacement of concrete overlay vary with the variation of t and a.

Hence, it can be concluded that adjusting parameter a holds greater significance in managing the maximum tensile stress of the concrete overlay, while modifying parameter t plays a crucial role in controlling the maximum vertical displacement. These observations provide valuable insights for engineers and designers to optimize and fine-tune the values of parameters a and t, ensuring desirable stress and displacement performance of the concrete overlay in various structural applications.

Based on the analysis of Figures 10 and 11, it is evident that the independent size parameters for a single U-rib include a, b, h, and t. However, to ensure compatibility between the BUSP and crossbeams, this study considers b as a constant value. Consequently, the dimensional parameters under investigation are a, h, and t. To explore the combined effects of these dimensional parameters on the stress of the concrete overlays, this study introduces the area parameter A for a single U-rib. This parameter, expressed by Equation (2) using the values of a, b, h, and t, plays a vital role in the analysis.

$$A = \frac{(a + 2y + b + 2x)h}{2} - \frac{(a + b)(h - t)}{2} \tag{2}$$

$$x = t/\tan\alpha \tag{3}$$

$$y = t/\sin(\pi - \alpha) \tag{4}$$

In Figure 22, the variation of the maximum tensile stress in the concrete overlays with respect to A is depicted. Notably, as the value of A increases, the maximum tensile stress in the concrete overlays initially decreases, reaching a minimum at approximately $A = 11,000$ mm^2, before subsequently increasing.

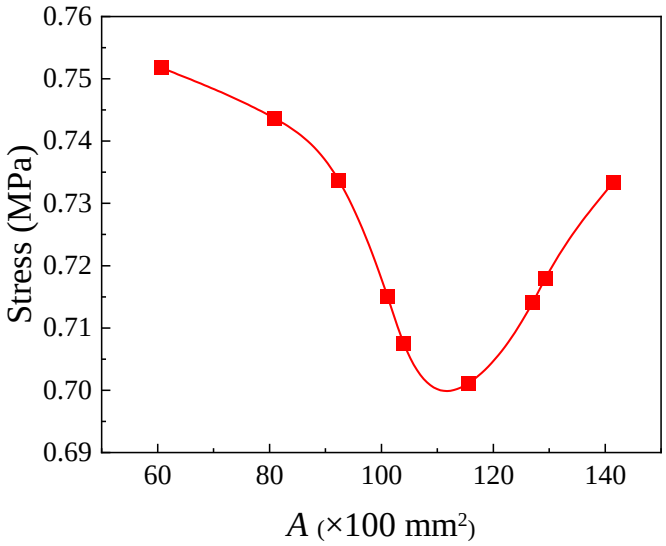


Figure 22. The variation of the maximum tensile stress in the concrete overlays with respect to A.

4.4. Influence of Spacing Parameters (e and w)

Distinguished from the size parameters of a single U-rib, the overall structural stiffness of the entire BUSP can be directly modified by adjusting the spacing parameters, thus enhancing its load-bearing performance. By reducing the spacing parameter e, the number of U-ribs along the longitudinal direction of the BUSP increases, leading to an improvement in its longitudinal stiffness. Similarly, by decreasing the spacing parameter w, the number of U-ribs along the transverse direction of the bridge increases, bolstering the bending stiffness in that direction.

To investigate the effects of these spacing parameters, three distinct models with varying parameters were constructed, as depicted in Figure 23. Model 1 represents the original structure of the BUSP, while Model 2 reduces the value of w to half of the original structure. In Model 3, the value of e is halved compared to the original structure. Model 4 simultaneously reduces both e and w to half of their original values.

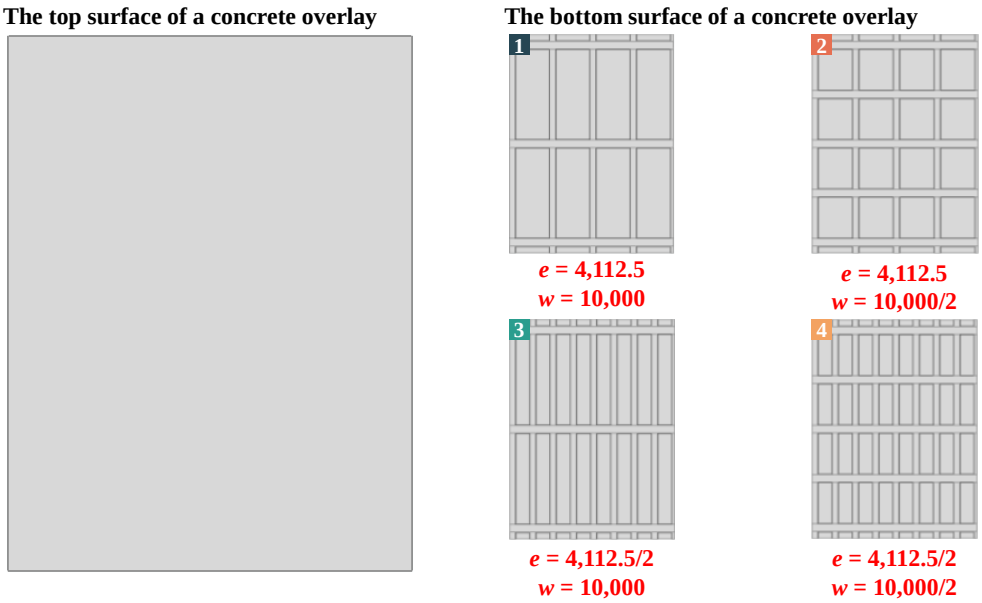


Figure 23. The models with varying spacing parameters (unit: mm).

The establishment of these models enables a comprehensive examination of the impact of spacing parameters on the overall stiffness of the BUSP. This investigation serves to inform engineers and designers seeking to optimize the structural performance and load-bearing capacity of the BUSP in different spatial orientations.

Figure 24 presents a comprehensive comparison of the maximum tensile stress in the concrete overlay among four different models, each with varying spacing parameters for both Structure 1 and Structure 2. From the graph, it is evident that adjusting the spacing parameters e and w leads to a notable decrease in the maximum tensile stress within the concrete overlay. Additionally, this reduction proves to be significantly more effective compared to modifying the dimensions of a single U-rib. Notably, by reducing the values of e and w, the stress levels near the transverse side span of the bridge are notably improved. This improvement becomes even more pronounced when increasing the number of transverse U-ribs (achieved by reducing the value of w).

These findings emphasize the importance of optimizing the spacing parameters in enhancing the stress distribution and performance of the concrete overlay. Engineers and designers can utilize this information to create more resilient and robust structures, particularly in areas prone to high tensile stress concentrations near the transverse side span of the bridge.

By analyzing Figure 24, it becomes apparent that adjusting the spacing parameters to alter the number of U-ribs in the concrete overlay leads to a corresponding shift in the location of the maximum tensile stress within the overlay. The specific positioning of this stress is showcased in Figure 25, which highlights the variations resulting from different spacing parameter configurations across both Structure 1 and Structure 2.

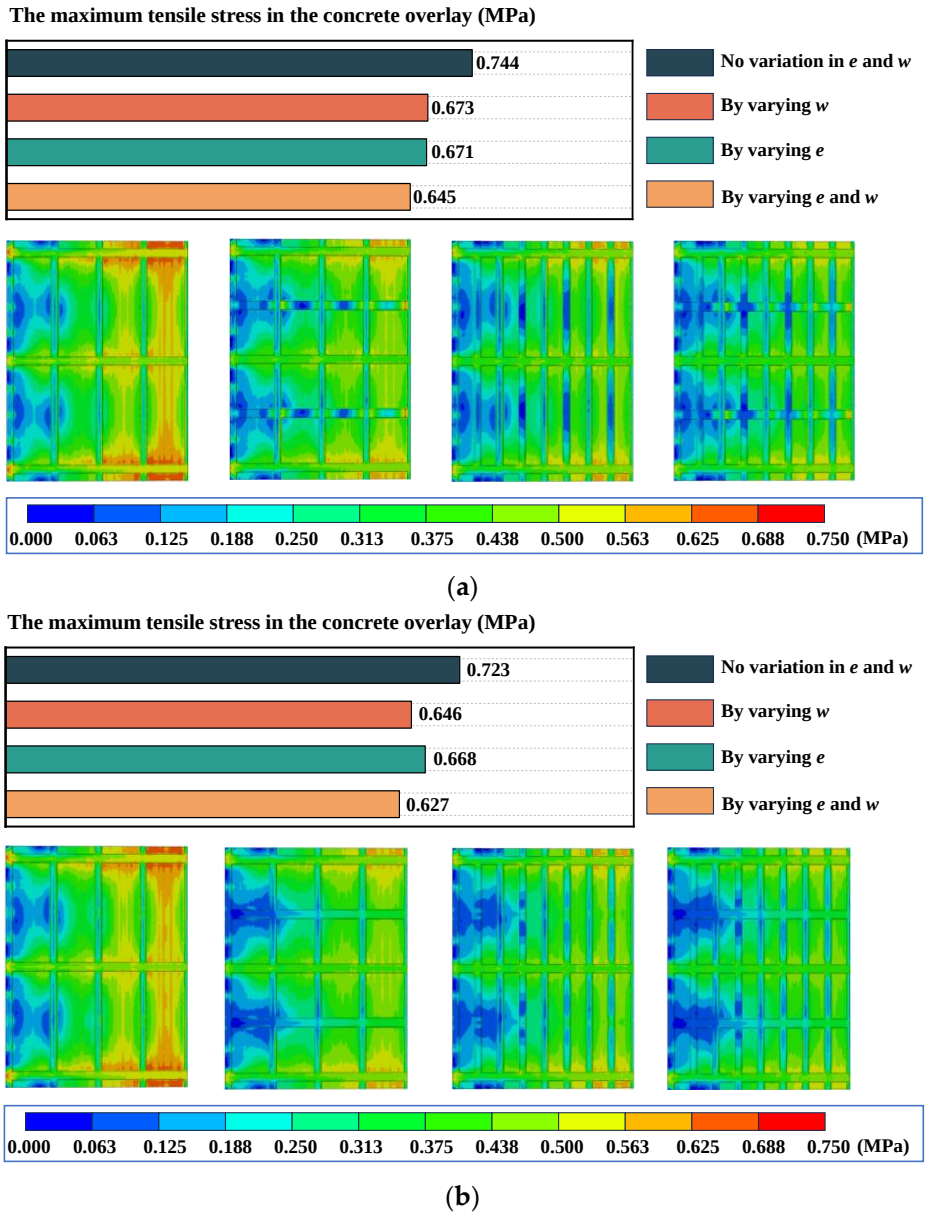


Figure 24. Stress distribution inside the concrete overlay: (**a**) structure 1, (**b**) structure 2.

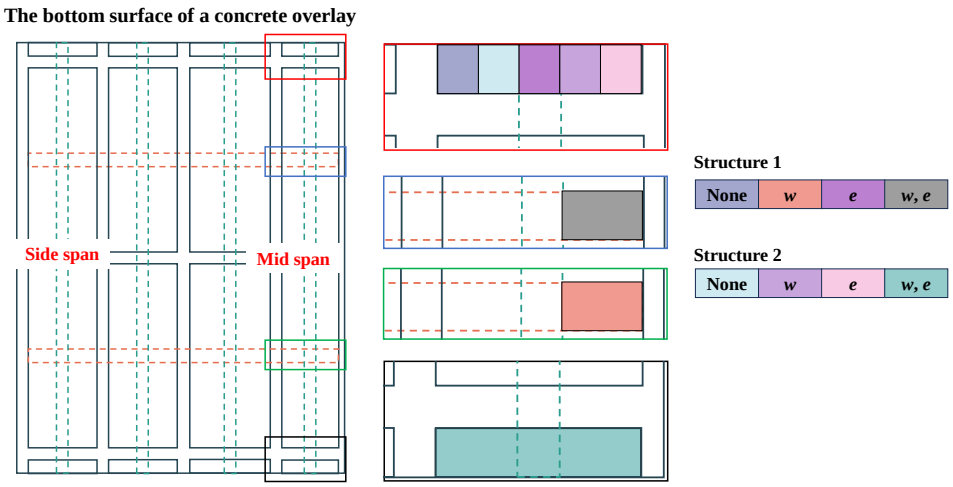


Figure 25. The location of the maximum tensile stress in the concrete overlay.

For a comprehensive examination, each structure includes four distinct spacing parameter setups for the BUSP. These configurations consist of the original BUSP structure, the BUSP structure with modified parameter w, the BUSP structure with modified parameter e, and the BUSP structure with simultaneous modifications to parameters w and e.

These visual representations offer valuable insights into the relationship between spacing parameters and the distribution of tensile stress within the concrete overlay. Engineers and researchers can utilize this knowledge to strategically optimize the design and placement of U-ribs to effectively manage stress concentrations in different regions of the BUSP.

The eight different models representing the four types of BUSP for both structures are visually distinguished by the eight colors displayed in Figure 25. From this figure, several significant conclusions can be drawn.

(a) The maximum tensile stress occurs at the mid-span of the bridge, which can be attributed to the peak bending moment experienced at this location.
(b) Keeping the values of parameters e and w constant, the original BUSP design shows that the maximum tensile stress in the concrete overlays for both Structure 1 and Structure 2 is located outside the U-rib stiffening region.
(c) Concerning Structure 1, altering parameter w, i.e., increasing the number of transverse U-ribs, results in a shift of the maximum tensile stress towards the added transverse U-ribs. However, changes in parameter e mainly affect the magnitude of the maximum tensile stress, while its location remains similar to the original BUSP design.
(d) For Structure 2, variations in parameters e and w primarily impact the magnitude of stress rather than its distribution. This distinction is primarily due to the support provided by the secondary beams in the crossbeam system of Structure 2 to the newly added transverse U-ribs, leading to different characteristics when compared to Structure 1.

Furthermore, Figure 26 demonstrates that the maximum vertical displacement of the concrete overlay also decreases as parameters e and w are reduced, following a similar pattern to the variation observed in maximum tensile stress.

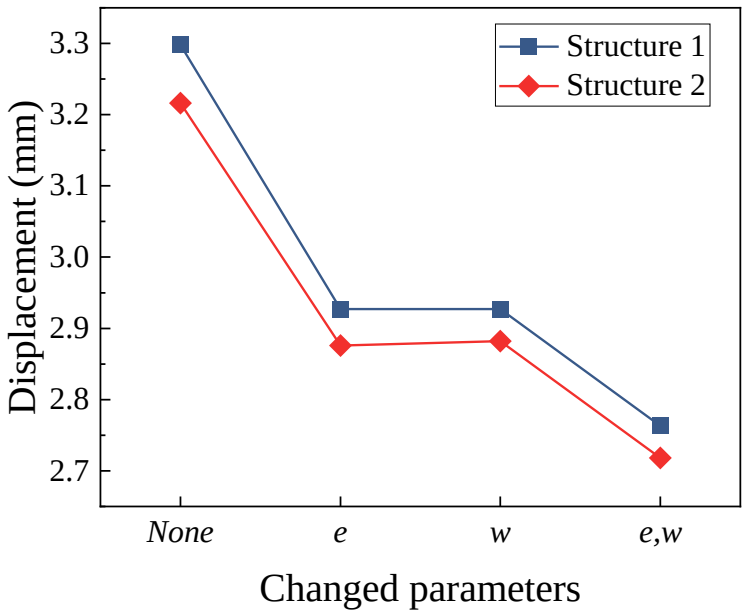


Figure 26. The maximum vertical displacement of the concrete overlay varies with the changes in parameters e and w.

These findings provide valuable insights into the behavior and performance of the BUSP under different spacing parameter configurations, enabling engineers to make in-

formed decisions in optimizing these parameters to minimize stress and displacement in concrete overlays.

5. Conclusions

In this study, a novel BUSP-concrete composite bridge deck system was designed. To analyze the impact of size parameters on its mechanical performance, a Python-based ABAQUS parameterized modeling script was developed. Based on the presented results, the following conclusions can be drawn.

- To achieve cast-in-place construction for the concrete structure of the bridge deck while maintaining the amount of steel used, thin steel plates were added to the original structure, and the crossbeam system was simplified. Finite element (FE) analysis demonstrated that the improved structure exhibited higher panel stiffness compared to the original design. Furthermore, the application of BUSP further increased the stiffness of the concrete overlay. Compared to the original design, it respectively reduced the maximum vertical displacement of the concrete overlay and the maximum tensile stress by 10.27% and 29.69%.
- When considering size parameters (h, t, and a) of a single U-rib of BUSP, it was observed that both the maximum tensile stress and maximum vertical displacement of the concrete overlay decrease with increasing t and a. Additionally, for h values not exceeding 100 mm, stress and displacement also decrease with increasing h. Compared to the original design, adjusting values of these three size parameters can reduce the maximum tensile stress of the concrete overlay by 15%. However, considering the quantities of steel and concrete used, adjusting the h value can be considered the most effective method for enhancing the mechanical performance of BUSP.
- By examining combinations of the three parameters (h, t, and a), their influence on the maximum tensile stress and maximum vertical displacement of the concrete overlay was compared. The research findings indicate that parameter a has the greatest impact on the stress of the concrete overlay, while parameter h has the greatest impact on vertical displacement.
- To investigate the combined effects of parameters h, t, and a, the parameter A, representing the area of the BUSP, was introduced. The results revealed that the minimum tensile stress of the concrete overlay is achieved when the value of A is approximately 11,000 mm^2.
- Reducing spacing parameters (e and w) can also enhance the mechanical performance of the BUSP. When only reducing the value of either e or w by half, the maximum vertical displacement and tensile stress of the concrete overlay can be reduced by approximately 10%. Furthermore, when simultaneously reducing the values of both e and w, the reduction magnitude can reach 15% or more. However, this improvement comes at the expense of increased construction difficulty and material expenses, as it requires the addition of extra U-ribs in the transverse or longitudinal direction of the bridge.
- These findings contribute to a better understanding of the mechanical behavior of BUSP and offer insights for optimizing its design parameters to enhance its performance while considering construction feasibility and cost-effectiveness.

Author Contributions: Conceptualization, F.H.; Methodology, J.L. (Jingwen Liao) and J.L. (Jianjun Liu); Validation, D.W. and Y.G.; Formal analysis, J.L. (Jingwen Liao); Writing—original draft, J.L. (Jingwen Liao); Writing—review & editing, Y.G. and F.H.; Supervision, J.L. (Jianjun Liu); Project administration, D.W. and F.H.; Funding acquisition, D.W. and F.H. All authors have read and agreed to the published version of the manuscript.

Funding: This work is supported by Guizhou Transportation Planning Survey & Design Academe (project no. ZLKY2023005).

Institutional Review Board Statement: Not applicable.

Informed Consent Statement: Not applicable.

Data Availability Statement: Data will be made available on request.

Acknowledgments: The authors would like to express their sincere gratitude to Pan Wang for his invaluable comments that have greatly enhanced the quality of this paper.

Conflicts of Interest: The authors declare no conflict of interest.

References

1. Kong, F.; Huang, P.; Han, B.; Wang, X.; Liu, C. Experimental study on behavior of corrugated steel-concrete composite bridge decks with MCL shape composite dowels. *Eng. Struct.* **2021**, *227*, 111399. [CrossRef]
2. Li, F.; Liu, B.; Sun, H.; He, W.; Wang, X. A novel corrugated steel plate-rubberized concrete composite slab: Properties and application opportunities. *Structures* **2022**, *43*, 1492–1502. [CrossRef]
3. Nie, J.; Wang, J.; Gou, S.; Zhu, Y.; Fan, J. Technological development and engineering applications of novel steel-concrete composite structures. *Front. Struct. Civ. Eng.* **2019**, *13*, 1–14. [CrossRef]
4. Zhang, H.-S.; Zhao, Y.; Ruan, J.; Nie, X.; Fan, J.-S.; Liu, Y.-F. Experiment study on temperature field and effect on steel-concrete composite bridge towers. *Structures* **2023**, *50*, 937–953. [CrossRef]
5. Zhang, Z.; Liu, Y.; Liu, J.; Xin, G.; Long, G.; Zhang, T. Experimental study and analysis for the long-term behavior of the steel–concrete composite girder bridge. *Structures* **2023**, *51*, 1305–1327. [CrossRef]
6. Briseghella, B.; Fa, G.; Aloisio, A.; Pasca, D.; He, L.; Fenu, L.; Gentile, C. Dynamic characteristics of a curved steel–concrete composite cable-stayed bridge and effects of different design choices. *Structures* **2021**, *34*, 4669–4681. [CrossRef]
7. Du, H.; Pan, J.; Shen, H.; Dong, J. Numerical Analysis of Flexural Behavior of Prestressed Steel-Concrete Continuous Composite Beams Based on BP Neural Network. *Comput. Intell. Neurosci.* **2022**, *2022*, 5501610. [CrossRef]
8. Uy, B.; Craine, S. Static flexural behaviour of externally post-tensioned steel-concrete composite beams. *J. Adv. Struct. Eng.* **2004**, *7*, 1–20. [CrossRef]
9. Ding, J.; Li, Y.; Xing, W.; Ren, P.; Kong, Q.; Yuan, C. Mechanical properties and engineering application of single-span steel-concrete double-sided composite beams. *J. Build. Eng.* **2021**, *40*, 102644. [CrossRef]
10. Sebastian, W.M.; McConnel, R.E. Nonlinear FE analysis of steel-concrete composite structures. *J. Struct. Eng.* **2000**, *126*, 662–674. [CrossRef]
11. Cheng, Z.; Zhang, Q.; Bao, Y.; Deng, P.; Wei, C.; Li, M. Flexural behavior of corrugated steel-UHPC composite bridge decks. *Eng. Struct.* **2021**, *246*, 113066. [CrossRef]
12. Sun, G.; Wang, Y.; Yang, J.; Chen, S.; Liu, H.; Zhao, J. Lightweight design method of orthotropic steel bridge deck with U-ribs based on multi-objective optimization. *Ain Shams Eng. J.* **2023**, 102464. [CrossRef]
13. Zhang, Q.; Bu, Y.; Li, Q. Review on fatigue problems of orthotropic steel bridge deck. *China J. Highw. Transp.* **2017**, *30*, 14–30. [CrossRef]
14. Deng, E.-F.; Zhang, Z.; Zhang, C.-X.; Tang, Y.; Wang, W.; Du, Z.-J.; Gao, J.-P. Experimental study on flexural behavior of UHPC wet joint in prefabricated multi-girder bridge. *Eng. Struct.* **2023**, *275*, 115314. [CrossRef]
15. Hattori, M.; Tateishi, K.; Hanji, T.; Shimizu, M. Fatigue strength evaluation by measurable stresses for root cracks in U-ribs to deck welded joints of orthotropic steel decks. *Weld World* **2023**, *67*, 2273–2282. [CrossRef]
16. Wu, W.; Kolstein, H.; Veljkovic, M. Fatigue resistance of rib-to-deck welded joint in OSDs, analyzed by fracture mechanics. *J. Constr. Steel Res.* **2019**, *162*, 105700. [CrossRef]
17. Cheng, X.; Fisher, J.W.; Prask, H.J.; Gnäupel-Herold, T.; Yen, B.T.; Roy, S. Residual stress modification by post-weld treatment and its beneficial effect on fatigue strength of welded structures. *Int. J. Fatigue* **2003**, *25*, 1259–1269. [CrossRef]
18. Cui, C.; Zhang, Q.; Luo, Y.; Hao, H.; Li, J. Fatigue reliability evaluation of deck-to-rib welded joints in OSD considering stochastic traffic load and welding residual stress. *Int. J. Fatigue* **2018**, *111*, 151–160. [CrossRef]
19. Shi, Z.; Yang, S.; Pu, Q.; Zhang, Y. Fatigue performance of orthotropic steel decks in long-span cable-stayed steel-box girder railway bridges. *J. Bridge Eng.* **2019**, *24*, 04019035. [CrossRef]
20. Chen, S.; Huang, Y.; Gu, P.; Wang, J.-Y. Experimental study on fatigue performance of UHPC-orthotropic steel composite deck. *Thin Walled Struct.* **2019**, *142*, 1–18. [CrossRef]
21. Fu, Z.; Wang, Y.; Ji, B.; Jiang, F. Effects of multiaxial fatigue on typical details of orthotropic steel bridge deck. *Thin Walled Struct.* **2019**, *135*, 137–146. [CrossRef]
22. Zhu, Z.; Li, J.; Chen, X.; Carpinteri, A. Stress behaviors of rib-to-deck double-sided weld detail on orthotropic steel deck. *J. Constr. Steel Res.* **2021**, *187*, 106947. [CrossRef]
23. Liu, Y.; Chen, F.; Lu, N.; Wang, L.; Wang, B. Fatigue performance of rib-to-deck double-side welded joints in orthotropic steel decks. *Eng. Fail. Anal.* **2019**, *105*, 127–142. [CrossRef]
24. Luo, P.; Zhang, Q.; Bao, Y.; Bu, Y. Fatigue performance of welded joint between thickened-edge U-rib and deck in orthotropic steel deck. *Eng. Struct.* **2019**, *181*, 699–710. [CrossRef]
25. Zhang, Z.; Tian, C.-K.; Deng, E.-F.; Peng, X.; Hu, H.-Y.; Li, F.-R. Fatigue performance and optimal design of corrugated steel–concrete composite bridge deck. *Structures* **2023**, *48*, 427–437. [CrossRef]

26. Ji, B.; Liu, R.; Chen, C.; Maeno, H.; Chen, X. Evaluation on root-deck fatigue of orthotropic steel bridge deck. *J. Constr. Steel Res.* **2013**, *90*, 174–183. [CrossRef]
27. Shao, X.; Yi, D.; Huang, Z.; Zhao, H.; Chen, B.; Liu, M. Basic performance of the composite deck system composed of orthotropic steel deck and ultrathin RPC layer. *J. Bridge Eng.* **2013**, *18*, 417–428. [CrossRef]
28. Yuan, Y.; Wu, C.; Jiang, X. Experimental study on the fatigue behavior of the orthotropic steel deck rehabilitated by UHPC overlay. *J. Constr. Steel Res.* **2019**, *157*, 1–9. [CrossRef]
29. Shemirani, A.B. Experimental and numerical studies of concrete bridge decks using ultra high-performance concrete and reinforced concrete. *Comput. Concr.* **2022**, *29*, 407–418.
30. Kim, H.-Y.; Jeong, Y.-J. Experimental investigation on behaviour of steel–concrete composite bridge decks with perfobond ribs. *J. Constr. Steel Res.* **2006**, *62*, 463–471. [CrossRef]
31. Machacek, J.; Cudejko, M. Longitudinal shear in composite steel and concrete trusses. *Eng. Struct.* **2009**, *31*, 1313–1320. [CrossRef]
32. Li, Y.; Liu, Y.; Liu, R. Finite element analysis on axial compressive behaviors of high-performance steel stiffened plates in bridge application. *Int. J. Steel Struct.* **2019**, *19*, 1624–1644. [CrossRef]
33. Oh, C.-K.; Hong, K.-J.; Bae, D.; Do, H.; Han, T. Analytical and experimental studies on optimal details of orthotropic steel decks for long span bridges. *Int. J. Steel Struct.* **2011**, *11*, 227–234. [CrossRef]
34. Chen, Z.-Y.; Li, C.-X.; He, J.; Xin, H.-H. Retrofit fatigue cracked diaphragm cutouts using improved geometry in orthotropic steel decks. *Appl. Sci.* **2020**, *10*, 3983. [CrossRef]

Disclaimer/Publisher's Note: The statements, opinions and data contained in all publications are solely those of the individual author(s) and contributor(s) and not of MDPI and/or the editor(s). MDPI and/or the editor(s) disclaim responsibility for any injury to people or property resulting from any ideas, methods, instructions or products referred to in the content.